2006

Evaluation of fraction of absorbed photosynthetically active radiation products for different canopy radiation transfer regimes: Methodology and results using Joint Research Center products derived from SeaWiFS against ground-based estimations

Nadine Gobron
Institute for Environment and Sustainability

Bernard Pinty
Institute for Environment and Sustainability

Ophélie Aussedat
Institute for Environment and Sustainability

Jing M. Chen
University of Toronto

Warren B. Cohen
USDA Forest Service

See next page for additional authors

Evaluation of fraction of absorbed photosynthetically active radiation products for different canopy radiation transfer regimes: Methodology and results using Joint Research Center products derived from SeaWiFS against ground-based estimations

Nadine Gobron,[1] Bernard Pinty,[1] Ophélie Aussedat,[1] Jing M. Chen,[2] Warren B. Cohen,[3] Rasmus Fensholt,[4] Valery Gond,[5] Karl Fred Huemmrich,[6,7] Thomas Lavergne,[1] Frédéric Mélin,[1] Jeffrey L. Privette,[6] Inge Sandholt,[4] Malcolm Taberner,[1] David P. Turner,[8] Michel M. Verstraete,[1] and Jean-Luc Widlowski[1]

Received 18 July 2005; revised 6 March 2006; accepted 30 March 2006; published 15 July 2006.

[1] This paper discusses the quality and the accuracy of the Joint Research Center (JRC) fraction of absorbed photosynthetically active radiation (FAPAR) products generated from an analysis of Sea-viewing Wide Field-of-view Sensor (SeaWiFS) data. The FAPAR value acts as an indicator of the presence and state of the vegetation and it can be estimated from remote sensing measurements using a physically based approach. The quality of the SeaWiFS FAPAR products assessed in this paper capitalizes on the availability of a 6-year FAPAR time series over the full globe. This evaluation exercise is performed in two phases involving, first, an analysis of the verisimilitude of the FAPAR products under documented environmental conditions and, second, a direct comparison of the FAPAR values with ground-based estimations where and when the latter are available. This second phase is conducted following a careful analysis of problems arising for performing such a comparison. This results in the grouping of available field information into broad categories representing different radiative transfer regimes. This strategy greatly helps the interpretation of the results since it recognizes the various levels of difficulty and sources of uncertainty associated with the radiative sampling of different types of vegetation canopies.

Citation: Gobron, N., et al. (2006), Evaluation of fraction of absorbed photosynthetically active radiation products for different canopy radiation transfer regimes: Methodology and results using Joint Research Center products derived from SeaWiFS against ground-based estimations, *J. Geophys. Res.*, *111*, D13110, doi:10.1029/2005JD006511.

1. Introduction

[2] The fraction of absorbed photosynthetically active radiation (FAPAR) has been recognized as one of the fundamental terrestrial state variables in the context of global change sciences [*Steering Committee for GCOS*, 2003]. It is a key quantity in models assessing vegetation primary productivity and, more generally, in carbon cycle models implementing up-to-date land surface process schemes [e.g., *Sellers et al.*, 1997; *Pitman*, 2003; *Knorr et al.*, 2005]. Establishing long-term time series of geophysical products, such as FAPAR, that are relevant for global scale applications calls for the use and interpretation of the remote sensing measurements collected by multiple sensors. Within this framework, *Gobron et al.* [2000] proposed a generic scheme and presented results from sensor specific algorithms that are devoted to the generation of equivalent, and thus comparable, FAPAR products derived from various optical sensors [*Gobron et al.*, 2006]. The concept underpinning these algorithms for deriving optimized vegetation indicators was proposed by *Verstraete and Pinty* [1996] and then applied to multiple sensors including, among others, the Medium Resolution Imaging Spectrometer (MERIS) [*Govaerts et al.*, 1999; *Gobron et al.*, 1999] and the Sea-viewing Wide Field-of-view Sensor (SeaWiFS) [*Gobron*

[1]Global Environmental Monitoring Unit, Institute for Environment and Sustainability, European Commission Joint Research Centre, Ispra, Italy.
[2]Department of Geography and Program in Planning, University of Toronto, Toronto, Ontario, Canada.
[3]USDA Forest Service, Corvallis, Oregon, USA.
[4]Institute of Geography, University of Copenhagen, Copenhagen, Denmark.
[5]Forest Department, Centre de Coopération Internationale en Recherche Agronomique pour le Développement, Cayenne, French Guyana.
[6]NASA Goddard Space Flight Center, Greenbelt, Maryland, USA.
[7]Now at Joint Research Center for Earth System Technology, University of Maryland Baltimore County, Baltimore, Maryland, USA.
[8]Department of Forest Science, Oregon State University, Corvallis, Oregon, USA.

0148-0227/06/2005JD006511$09.00

et al., 2001]. The MERIS FAPAR products have been derived operationally since the launch of the Envisat platform in March 2002 (see, for example, http://envisat.esa.int). The SeaWiFS FAPAR products are generated at the JRC thanks to a dedicated processing chain that was developed to deliver daily, 10-day and monthly composite products at a global scale with spatial resolutions ranging from about 2 km up to 0.5 degrees [*Mélin et al.*, 2002; *Knorr et al.*, 2005]. At the time of writing, 6 years of SeaWiFS FAPAR products are available from September 1997 (beginning of the mission) to December 2004. Such a multiannual global time series is quite suitable for conducting investigations aimed at assessing the performance of this category of FAPAR algorithms and the associated products they generate.

[3] The validation of geophysical products, such as FAPAR, derived from remote sensing data is required to evaluate whether the quality of these products conforms with the preflight specified accuracy, itself imposed by requirements from the anticipated series of applications. Space agencies have therefore developed their own calibration and validation projects on both atmospheric and land surfaces products (see, for example, http://envisat.esa.int, http://www-misr.jpl.nasa.gov/mission/valid.html and http://landval.gsfc.nasa.gov/MODIS/, among others). In the specific cases of the MODerate Resolution Imaging Spectroradiometer (MODIS) and the Multiangle Imaging SpectroRadiometer (MISR) sensors operating on board the Terra platform, significant efforts are devoted to the validation of surface products such as the leaf area index (LAI) and FAPAR generated from data acquired by these sensors [e.g., *Huemmrich et al.*, 2005; *Wang et al.*, 2004; *Shabanov et al.*, 2003]. The science strategy adopted for designing the MODIS and MISR LAI/FAPAR algorithms is such that the LAI product values need to be carefully evaluated since their determination impacts results of the FAPAR algorithm itself [e.g., *Knyazikhin et al.*, 1998a, 1998b]. Both LAI (a state variable of the radiation transfer problem) and FAPAR (a normalized radiant flux in the visible region of the solar domain) products correspond to physical quantities that can be measured in the field with different but significant levels of difficulty. Some of these difficulties for generating accurate ground-based estimations of FAPAR are addressed in section 4 of this paper. Given these difficulties, qualitative approaches can be considered in order to evaluate the capability of the satellite derived surface products to exhibit, at least, anticipated signatures of well-identified geophysical events. These approaches thus include the analysis of the FAPAR (and LAI) time series over geographical regions where the vegetation cycles are mainly controlled by human activities, as is the case for agricultural crops, as well as where the occurrence of drought, fire and heavy rainfall events have been reported.

[4] The second section of this paper briefly describes the main features of the SeaWiFS (and MERIS) FAPAR algorithms and gives a short description of the associated FAPAR products. The third section highlights the ability of the FAPAR products to exhibit meaningful signatures of vegetation processes with or without the occurrence of stressing events. The comparison between remote sensing and ground-based estimations of FAPAR is presented in a fourth section. Issues related to the internal variability of the studied systems and expected consequences on the representativity of the ground-based estimations are first extensively analyzed. This leads to a categorization of the few ground-based FAPAR data sets according to their most probable radiative transfer regimes. The evaluation of the comparison results is thus associated with the contextual difficulties shown by each specific site and the corresponding data sets. A concluding section summarizes the findings.

2. Overview of the FAPAR Algorithm and FAPAR JRC Products Derived From SeaWiFS

[5] The JRC generic FAPAR algorithm can be tailored to any sensor acquiring at least three spectral bands in the blue, red and near-infrared regions of the solar spectrum. This algorithm capitalizes on the physics of remote sensing measurements and its development copes with the many operational constraints associated with the systematic processing and analysis of a large amount of data. Basically, the useful information on the presence and state of vegetation is derived from the red and the near-infrared spectral band measurements. The information contained in the blue spectral band, which is very sensitive to aerosol load, is ingested in order to account for atmospheric effects on these measurements.

[6] In the specific cases of the SeaWiFS and MERIS sensors, which were primarily designed for marine applications, neither the MODIS strategy, exploiting the availability of the 2.1 μm spectral band [e.g., *Kaufman et al.*, 1997, 2002], nor the MISR approach [e.g., *Martonchik et al.*, 1998], using simultaneous multiangle measurements, can be adopted for atmospheric correction purposes. In the mean time, operational constraints impose the necessity to generate reliable products on a pixel and single orbit basis. Our original approach thus consists in analyzing the relationships between measurements in the blue spectral band and those available in the red and near-infrared regions [e.g., *Govaerts et al.*, 1999; *Gobron et al.*, 1999]. Such relationships can indeed be simulated for a variety of environmental conditions with radiation transfer models of the coupled vegetation-atmosphere system. The former are then exploited with polynomial expressions optimized in such a way that top of atmosphere bidirectional reflectance factor (BRF) measurements in the blue are related to those taken at other spectral bands, located at longer wavelengths, for example, in the red and near-infrared regions. This approach aims at decontaminating the BRFs from atmospheric effects without performing an explicit retrieval of the ambient atmospheric properties. The polynomial expressions are also built to simultaneously account for the bulk of the anisotropy effects. The latter are themselves approximated from an extensive set of one-dimensional radiation transfer simulations of the coupled surface-atmosphere system designed for mimicking typical vegetation canopy conditions [*Gobron et al.*, 2000]. This same training data set is then used to relate the radiative measurements from each typical vegetation canopy condition to their corresponding FAPAR values. Strong three-dimensional effects may affect to some extent the accuracy of the products retrieved by the FAPAR algorithm. The latter was, however, shown to be

quite robust with respect to specific perturbations induced by such three-dimensional effects [*Gobron et al.* 2000, section 4-b]. As demonstrated by *Widlowski et al.* [2005], one-dimensional models can almost always mimic reflectances generated by three-dimensional models providing the former category implements appropriate state variable values. As a matter of fact, the range of values adopted when designing the training data set for the FAPAR algorithm has to be large enough to include such combinations of appropriate values.

[7] In practice, the generic FAPAR algorithm thus implements a two-step procedure where the spectral BRFs measured in the red and near-infrared bands are, first, rectified in order to ensure their optimal decontamination from atmospheric and angular effects and, second, combined together to estimate at best the instantaneous FAPAR value at the time of acquisition. The most recent versions of the appropriate formulae and coefficients, optimized and thus prototyped to account for each specific instrument characteristics, derived from the mathematical optimization are given by *Gobron et al.* [2002] for SeaWiFS and *Gobron et al.* [2006] for MERIS, respectively.

[8] All results discussed in this paper are derived from the SeaWiFS FAPAR algorithm that has been applied on all available data acquired by the SeaWiFS sensor, in operation since autumn 1997. On board the Orbview-2 spacecraft, the SeaWiFS sensor [*Hooker et al.*, 1992] collects measurements in eight narrow spectral bands extending from the blue to the near-infrared region of the solar spectrum, ensuring a daily global coverage approximately every 2 days. SeaWiFS raw data (both so-called Global and Local Area Coverage) were originally provided in the orbital projection by NASA GSFC to JRC. The actual spatial resolution of the geophysical products depends therefore on the nominal pixel size which is changing across track and has been remapped into a global sinusoidal projection at 2.17 km resolution using a nearest neighbor technique [*Mélin et al.*, 2002]. The following analysis has been conducted using FAPAR values extracted from this global data set, from either daily samples or a 10-day composite time period. The time composite algorithm of *Pinty et al.* [2002] has been applied on the sequence of daily FAPAR products to provide representative values of each time period. These representative values are selected so that they correspond to the closest values to the corresponding arithmetic averages of the daily FAPAR values calculated over each time period. The FAPAR algorithm was originally designed and implemented in order to generate, at medium spatial resolution, daily FAPAR products whose absolute accuracy remains statistically within the pre-specified ±0.1 range. This range should permit us to reliably detect significant FAPAR signatures of a variety of environmental events occurring on land surfaces. It also acknowledges the complexity of comparing medium resolution FAPAR products derived from remote sensing with corresponding ground-based estimations [*Widlowski et al.*, 2006]. The quality assessment of the SeaWiFS FAPAR JRC products described below concentrates on conditions where the illumination conditions do not significantly exceed those adopted in the algorithm training data set, that is 50° in Sun zenith angle. The difficult case of high latitude ecosystems, such as boreal coniferous forests, is thus excluded from the present exercise.

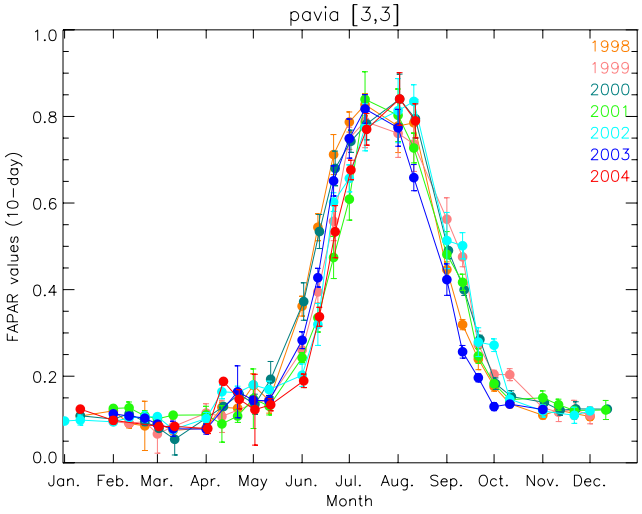

Figure 1. Time series of 10-day composite SeaWiFS FAPAR JRC products, spatially averaged over 3 × 3 pixels, that is, about 6 × 6 km^2, over rice cultivation close to Pavia, Italy (45°17′N; 8°23′E). The error bars correspond to the spatial standard deviation around the central pixel.

3. Analysis of FAPAR Times Series

[9] The results presented in this section derive from the analysis of 6 years of FAPAR times series over three different land cover types to illustrate the signal variability due to the vegetation seasonal cycles as well as the signatures resulting from the occurrence of environmental stress, i.e., drought and fire events. Figure 1 illustrates the signature of the FAPAR products in response to the seasonal cycle occurring over rice cultivation close to Pavia, Italy (45°17′N; 8°23′E). The FAPAR values shown in this figure correspond to the 10-day time composite products spatially averaged over 3 × 3 pixels, that is about 6 × 6 km^2, around the central pixel. The error bars show the standard deviation over the 3 × 3 pixels, thus indicating the current spatial variability around the site. The FAPAR time series from 1998 to 2004 indicate very similar phenological cycles over the various years as expected for such agricultural fields in which water availability is essentially controlled by irrigation. Rice grows from April onward and reaches maturity in July/August associated with series of maxima in the FAPAR values. From September onward, harvesting is accompanied by a sharp decrease in FAPAR. The strong seasonal cycles are quite similar during these 6 years although, owing to an earlier growth in spring 2003, the FAPAR values are exhibiting an earlier decrease in 2003 as compared to other years. This example thus shows that the SeaWiFS FAPAR products are capable of monitoring well-defined seasonal cycles in a quite reproducible manner.

[10] The time series shown in Figure 2 corresponds to FAPAR values over the Pearsoll Peak site located in Oregon, United States (42°18′N; 123°51′W) which is covered by wild forest. The FAPAR values are very stable from 1998 to 2001 and then show a quite sudden and dramatic

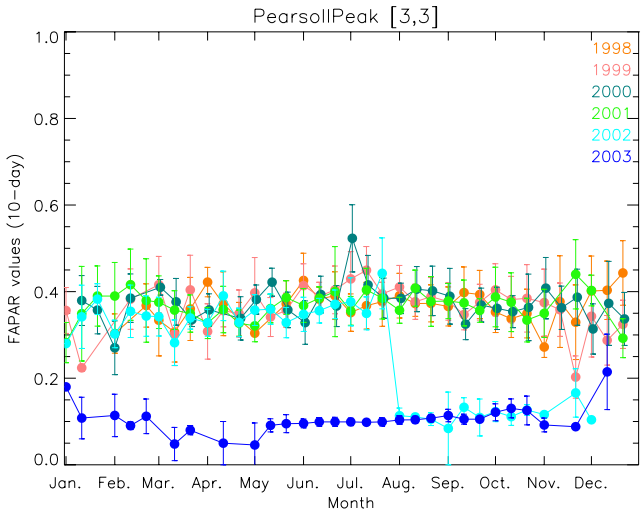

Figure 2. Time series of 10-day composite SeaWiFS FAPAR JRC products, spatially averaged over 3 × 3 pixels, that is, about 6 × 6 km^2, over Pearsoll Peak, Oregon, United States (42°18′N; 123°51′W). The error bars correspond to the spatial standard deviation around the central pixel.

drop from about 0.4 to 0.1 in August 2002, in response to an intense fire event reported by the USDA Forest Service (http://www.fs.fed.us/). Low values observed during year 2003 suggest that the vegetation was not able to recover from this extreme stress event. In addition to the results displayed in Figure 1, the FAPAR products are thus capable of detecting and documenting major perturbations in the vegetation cover at the Earth's surface.

[11] The next example (Figure 3) exhibits FAPAR time series estimated over one of the main sites of the CARBOEUROPE Integrated Project (http://www.carboeurope.org/). This site, equipped in order to perform exhaustive measurements for monitoring the carbon cycle, is located close to the city of Hesse, France (48°40′N; 07°04′E). The dominant land cover type surrounding the central site location (the geographical coordinates of the latter are taken from the location of the measuring tower) is hardwood beech forest (*Fagus sylvatica*) although other tree species (*Quercus petrea* and *Betula alba*) and canopy understory have been inventoried on this site (http://www-bcg-jena-mpg.de/public/carboeur/sites/). This time series of FAPAR shows typical seasonal cycles over this hardwood forest site, in response to its dominant phenological activity. The photosynthetic activity increases from April and exhibits a first peak in May, followed by a slight decrease until July/August and then a second decrease during the fall season associated with the senescence period and the yellowing of the leaves [*Wang et al.*, 2005]. Although the FAPAR signature appears somewhat noisier than for irrigation controlled agricultural sites (as in Figure 1, for instance), the interannual variability remains limited under normal environmental conditions. Such a variability has been already observed in the field and associated with a year-to-year changing rate of decrease in the LAI [*Wang et al.*, 2005]. By contrast, the FAPAR values estimated for year 2003 are abnormally low as compared to previous years, owing to the exceptionally strong stress imposed on vegetation as a consequence of a drought event and summer heat wave [*Gobron et al.*, 2005]. The FAPAR time series over this beech forest also suggests that vegetation was still or again affected in mid to late summer 2004 since FAPAR did not fully recover the average level from previous years.

[12] The three selected and highly contrasting examples that were discussed in this section highlight the capability of the SeaWiFS FAPAR JRC products for exposing a variety of signatures in response to the vegetation health and state. The results of this analysis therefore provide some confidence in the performance of these FAPAR products and confirm their capability to detect regional [*Gobron et al.*, 2005] and global scale environmental perturbations [*Knorr et al.*, 2005]. The observed anomalies of the seasonal cycles following a stress event appear significant in regard to the noise level inherent to the FAPAR algorithm and the natural variability of the signal. The following section analyzes more thoroughly whether such performances are indeed reached on the basis of a series of available FAPAR ground-based estimations.

4. Comparison Against Ground-Based Estimations

[13] Comparing remote sensing products retrieved at medium spatial resolutions (pixel size of about 1 km in horizontal dimension or more) with in situ measurements implies addressing a number of issues and trade-offs. For instance, the uncertainty in the exact location of particular pixel coordinates on the Earth geoid when remapped, suggests averaging the values over a square of multiple grid points to ensure that the resulting time series relate to the same geophysical system. For their part, the protocols for acquiring local ground measurements must be such that they tend to minimize undesirable effects related to the different spatial resolutions between the retrieved remote sensing products and the ground-based measurements. Spe-

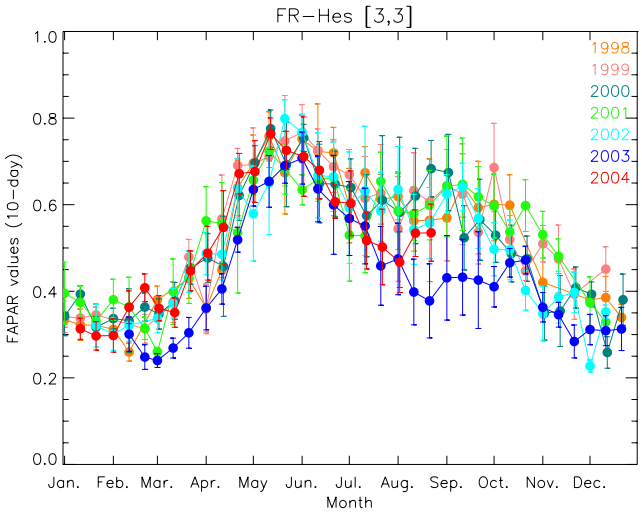

Figure 3. Time series of 10-day composite SeaWiFS FAPAR JRC products, spatially averaged over 3 × 3 pixels, that is, about 6 × 6 km^2, over Hesse, France (48°40′N; 07°04′E). The error bars correspond to the spatial standard deviation around the central pixel.

cifically, ground measurements must represent at best the three-dimensional (3-D) spatial variability of the canopy attributes and radiant fluxes existing inside the (relatively low resolution) sampled domain.

[14] In the present paper, we are dealing with SeaWiFS derived products remapped to a sinusoidal projection at a spatial resolution of 2.17×2.17 km^2, such that the analysis of FAPAR time series can be conducted, without performing a spatial aggregation, over pixels identified as the nearest to the nominal location of the measurement site. It also means that this resolution is slightly too coarse to fully ensure that the ground-based, eventually domain-averaged, measurements result from a complete spatial sampling at that same resolution. Over these selected pixels, time composite algorithms can be applied to eliminate outliers and to limit the impact of uncertainties inherent in the algorithm (e.g., remaining biases due to changing Sun and view geometries and/or un-foreseen atmospheric conditions), intermittent presence of sub-pixel clouds, or any other undesired events such as occasional water or snow during the composite period. For the present comparison exercise, daily and 10-day composite values will be used. In the next section, a number of issues concerning the difficulties in assessing domain-averaged FAPAR values are discussed and associated with different categories of radiation transfer regimes, themselves related to different types of vegetation canopies.

4.1. Ground-Based Estimations of Domain-Averaged Values

[15] Domain-averaged FAPAR (the absorbed flux fraction estimated over the photosynthetically active radiation (PAR) spectral region) is neither measured nor simulated directly as such: Its estimation results from the closure of an energy balance equation in the vegetation layer at the spatial resolution of the domain. Under direct illumination with cosine zenith angle μ_0, it is equal to

$$\mathrm{FAPAR}(\mu_0) = \left[1 + R_{bgd} \times T\left(z_{bgd}, \mu_0\right)\right] - \left[R(z_{toc}, \mu_0) + T\left(z_{bgd}, \mu_0\right)\right] + H(\mu_0), \quad (1)$$

where $R(z_{toc}, \mu_0)$ represents the albedo at the top of the canopy z_{toc} and $T(z_{bgd}, \mu_0)$ represents the total transmission (both the direct and diffuse components) at the bottom of the vegetation layer z_{bgd}. R_{bgd} denotes the albedo of the background underneath the vegetation layer, and $H(\mu_0)$ corresponds to the net effect (positive or negative) due to the horizontal fluxes through the lateral boundaries of the domain. Note that $T(z_{bgd}, \mu_0)$ includes the contributions due to scattering processes in the vegetation layer as well as those due the multiple interactions between the vegetation layer and the background [*Pinty et al.*, 2005]. All normalized radiant fluxes listed in (1) are domain-averaged quantities.

[16] Equation (1) asserts that the net horizontal flux, in addition to three domain-averaged fractions of vertical fluxes, needs to be known in order to estimate FAPAR. The technical difficulties associated with the in situ assessment of the vertical fluxes depend on the canopy attributes, including average height and spatial heterogeneity. For short vegetation canopies, on the one hand, the measurements of the fluxes impinging on the background and arising from the background are rather difficult; on the other hand, the albedo of the vegetation canopy and its spatial variability can be assessed relatively easily. By contrast, in the case of tall vegetation, it is the estimate of spatially representative albedo values of the vegetation canopy that is rather difficult, and especially the documentation of the spatial variability of this normalized flux. Depending on the size of the footprint of the measuring device, high enough towers sometimes offer appropriate support. However, it remains hard to guarantee that this device samples statistically all scales of variability exhibited by the vegetation layer, such that its measurements can be analyzed to estimate representative domain-averaged values to be used in (1). The downward transmitted flux and its spatial variability at specific scales and resolutions is technically easier to estimate below tall canopies [e.g., *Brown et al.*, 1994; *Comeau et al.*, 1998]. When this variability is large (e.g., large values of the variance (or higher moments) with respect to the mean), the estimation of representative domain-averaged fluxes is even more complicated [e.g., *Nicotra et al.*, 1999]. In these circumstances, it is difficult to ensure that the different sampling techniques used at the top and at the bottom of the vegetation layer lead to statistically consistent domain-averaged flux values needed for closing (1).

[17] When estimating FAPAR from medium or low spatial resolution sensors, the contribution due to the net radiant horizontal fluxes is negligible at any level with respect to the vertical fluxes [see *Widlowski et al.*, 2006]. For all practical purposes, the inverse algorithms implemented to interpret medium- and low-resolution remote sensing measurements can thus safely assume that $H(\mu_0) \rightarrow 0$. By the same token, these results also suggest that at local resolutions of less than a few meters, such as those involved when performing in situ measurements, the contribution from $H(\mu_0)$ (which is rarely or never measured in situ) can be quite significant, especially for tall and open canopies. This contribution has to be compared with the one due to the horizontal variability of the vertical fluxes. One of the challenges when performing ground validation experiments (with the condition $H(\mu_0) \rightarrow 0$) is to ensure that (1) the field measurements adequately sample the internal variability of the domain at the appropriate frequency (in the case of vegetation layers; this implies a sampling step corresponding to the typical inter-leaf/shoot distance); and (2) the sampled area is large enough so that the associated domain-averaged values are independent of the exact location of this sampled area within the vegetation system (i.e., deriving domain-averaged values that are representative of the system). For example, tall canopies with low leaf densities generally exhibit significant 3-D structure and hence a hierarchy of gaps where the internal variability of the leaf distribution function is quite high [e.g., *Parker*, 1995]. In such conditions, the horizontal extent of the domain sampled in the field must be several times the typical height of the canopies to reach conditions where the relative contribution of $H(\mu_0)$ with respect to the vertical fluxes is negligible.

[18] The joint estimation of the appropriate domain-averaged vertical and horizontal flux quantities entering (1) in the PAR spectral region is therefore crucially dependent on the sampling frequency and the size of the sampled domain

as well as the architectural attributes of the vegetation layer and the nature of the illuminating sources both at the upper (downward direct and diffuse sky radiation) and lower (upward radiation field scattered by the background) boundaries. For all practical purposes, the spatial variability of the leaf density prevailing inside the vegetation layer over the domain is one of the most delicate problems to be addressed both technically and statistically for accurately closing (1) on the basis of the individual flux contributions. As a consequence, one can anticipate that the accuracy level that can be reached when computing (1) genuinely depends on the level of statistical variability of the vegetation layer and the means to estimate it.

[19] The impacts of different types of internal variability of the extinction coefficient together with the resolution of the sampled domain on the radiation transfer regime for clouds was analyzed by *Davis and Marshak* [2004]. On the basis of theoretical arguments, these authors thoroughly established the conditions where 3-D effects are anticipated to play a major role in the establishment of the radiation transfer regime. Their results can be extrapolated to the case of land surfaces to help us to associate the main radiative transfer regimes with the statistical properties of the leaf extinction coefficient inside the spatial domain of investigation: (1) a ''fast'' variability regime in the case of statistically homogeneous, Poisson-like, distributions of the leaf density, (2) a ''slow'' variability regime where, in fact, the leaf density distribution is close enough to being homogeneous only locally such that local-scale average flux values are meaningful and (3) a ''resonant'' regime in other cases where the spatial complexity is such that a typical photon beam will sample different types of vegetation structures between entering and escaping the canopy, variability thus controls the domain-average fluxes. Such regimes correspond to an intrinsic radiative property of the canopies themselves as they interact with the flow of solar radiation. We will however exploit this identification scheme from the practical standpoint of a given spatial resolution.

[20] Canopies and resolutions favoring regimes 1 and 2 are simpler to deal with than those exhibiting regime 3 in the context of both performing in situ flux measurements and modeling the radiation transfer phenomena. Indeed, these former regimes basically call for the use of one-dimensional (1-D) theory to be applied either over the full domain (regime 1) or only ''locally'' and then extended over the full domain using linear mixing techniques (regime 2). In the case of regime 3, canopy structure is a major component of the problem and the 3-D heterogeneity controls a significant part of the domain-averaged flux values that are themselves neither easily estimated in the field nor modeled accurately, unless the statistics of the canopy elements are well known.

[21] For all practical purposes, short vegetation and tall but dense canopy layers tend to exhibit only small characteristic scales, close to the typical inter-leaf/shoot distance. If only one type of such vegetation exists in the studied domain for FAPAR, regime 1 prevails. When multiple types of vegetation/land cover exist inside the domain, a typical case for medium to low spatial resolution sensors, any vegetation storey must be sampled such that the average ''local'' flux values can be estimated in a statistically meaningful manner. The domain-averaged values are then generated by a straightforward spatial aggregation of the vegetation types, weighted by the fractional area inside the domain. Regime 2 may thus dominate, especially if the conditions for regime 1 are fulfilled ''locally'' over each individual land cover patch. One may logically expect that tall (favoring long horizontal displacement of radiation with respect to its origin of entry) and clustered (creating a hierarchy of small scale gaps) but not dense (permitting radiation to travel with small extinction probability) vegetation canopies exhibit the type of variability categorized in regime 3. The latter occurrence calls for a well-conceived measuring protocol [*Widlowski et al.*, 2006].

[22] In actual conditions, all sorts of combinations of such regimes coexist at medium and low spatial resolutions. Vegetation canopies are also composed of woody elements for which both statistical and radiative properties significantly differ from those of the leaves. Given the many caveats and difficulties associated with the accurate estimation of domain-averaged fluxes, the next section discusses some approximations that can be made to simplify the problem of comparing FAPAR values retrieved from remote sensing against those deduced from ground estimations of measurable fluxes and major canopy attributes. Such simplifications are needed to better understand the interpretation of the ground data sets selected for comparison, as well as to acknowledge up front some of their limitations.

4.2. Intercepted Radiation: A Proxy for FAPAR

[23] Since the fraction of absorbed flux is a function of the directionality of the illumination source, an equation similar to (1) holds for diffuse sky illumination and, to simplify the problem further, one can assume that FAPAR estimates from ground flux measurements, $\mathrm{FAPAR}^{\star}(\mu_0)$, are approximated by

$$\mathrm{FAPAR}^{\star}(\mu_0) \approx \mathrm{FAPAR}(\mu_0) f^{\downarrow dir}(\mu_0) + \overline{\mathrm{FAPAR}} f^{\downarrow diff}(\mu_0) \quad (2)$$

where the weights, $f^{\downarrow dir}$ and $f^{\downarrow diff}$, sum up to 1 and correspond to the fractions of direct and diffuse to total downward flux density, respectively. Equation (2) is based on the reasonable assumption that the FAPAR, as would be measured in the field under actual conditions of illumination, can be approximated by a linear combination of two FAPAR contributions: a directional-hemispherical flux, $\mathrm{FAPAR}(\mu_0)$, associated with a purely collimated incident intensity field, and a bihemispherical flux, $\overline{\mathrm{FAPAR}}$, associated with a purely isotropic incident intensity field. Such an approximation is largely used for approximating the albedo of land surfaces under ambient conditions [*Lewis and Barnsley*, 1994; *Pinty et al.*, 2005]. Equation (2) provides a means to estimate FAPAR under arbitrary sky conditions, provided that the vertical and horizontal fluxes in (1) can be estimated under direct and diffuse illumination separately.

[24] Since the single scattering regime (identified by a superscript 1 *s*) dominates the absorption process by vegetation in the PAR spectral region [see *Pinty et al.*, 2006] it is possible to rewrite (2) as follows:

$$\begin{aligned}\mathrm{FAPAR}^{\star\,1s}(\mu_0) \approx {} & \left(\mathrm{FIPAR}(\mu_0) + \delta_{A^{1s}}(\mu_0)\right) \cdot f^{\downarrow dir}(\mu_0) \\ & + \left(\overline{\mathrm{FIPAR}} + \overline{\delta_{A^{1s}}}\right) f^{\downarrow diff}(\mu_0) \end{aligned} \quad (3)$$

where the fluxes associated with the incoming diffuse sky illumination are identified by an overbar and where FIPAR(μ_0) denotes the fraction of direct radiation intercepted by the leaves only; that is,

$$\mathrm{FIPAR}(\mu_0) = 1 - T_{veg}^{UnColl}(\mu_0) \quad (4)$$

where the so-called uncollided transmission, T_{veg}^{UnColl}, denotes the direct transmission of solar radiation that has traveled downward through the canopy gaps only and thus has not suffered from any collision with canopy elements. A similar equation can be written with respect to the diffuse sky illumination.

[25] In the limit of single scattering regime and under direct illumination, $\delta_{A^{1s}}$ can be accurately approximated by [see *Pinty et al.*, 2006]

$$\begin{aligned}\delta_{A^{1s}}(\mu_0) &= \mathrm{FAPAR}^{\star 1s}(\mu_0) - \mathrm{FIPAR}(\mu_0) \\ &= R_{bgd}\, T_{veg}^{UnColl}(\mu_0)\left(1 - \overline{T_{veg}^{UnColl}}\right) - R_{veg}^{Coll1s}(z_{toc}, \mu_0); \quad (5)\end{aligned}$$

$\delta_{A^{1s}}$ is thus a function expressing the balance between the contributions due to the fraction of up-scattered flux at the top of the canopy, that is the albedo of the canopy, $R_{veg}^{Coll1\,s}$, (negative contribution), and the fraction of up-scattered flux at the bottom of the canopy (positive contribution). The latter is logically given by the product of the source term at the background level illuminating the vegetation canopy from below, $R_{bgd}T_{veg}^{UnColl}(\mu_0)$, and the intercepted fraction over the entire upward hemisphere, $(1 - \overline{T_{veg}^{UnColl}})$. A similar equation is obtained with respect to the diffuse sky illumination, by replacing the directional-hemispherical with their corresponding bihemispherical quantities in (5).

[26] As discussed in section 4.1, the estimate of radiant fluxes in both structurally heterogeneous and homogeneous vegetation canopies is rendered somewhat complex by the type of boundary conditions to be considered: direct and diffuse radiation at the top of the canopy and a reflecting background at the bottom. Note that this situation has been significantly simplified by assuming an isotropic diffuse sky illumination yielding the linear parameterization proposed in (2) for estimating the radiant fluxes. It can be further simplified if a Lambertian background is considered thus creating an isotropic source of radiation at the bottom of the canopy.

[27] Equation (5) highlights the role of the lower boundary condition which acts as an additional source of radiation to the vegetation layers and thus contributes positively to the absorption process. Its impact on the fraction of absorbed flux, $\delta_{A^{1s}}(\mu_0)$, has been estimated numerically for various background brightness conditions underlying a selection of canopy scenarios in the PAR spectral domain. The 3-D heterogeneous canopy scenarios used below are the same as those described by *Pinty et al.* [2006, Tables 1 and 2]. They correspond to sparse, medium and dense forest canopies with allometric domain-averaged LAI values, $\langle LAI \rangle$, equal to 1.24, 2.0 and 4.82, respectively.

[28] The values of $\delta_{A^{1s}}(\mu_0)$ are displayed in Figure 4 as a function of the background brightness, R_{bgd}. The leaf absorption efficiency is such that for dense canopy conditions, the $\delta_{A^{1s}}(\mu_0)$ function values remain close to zero for almost any background condition. Since the decrease in $\langle LAI \rangle$ is accompanied by a higher probability for the solar radiation to reach the background, the effect of the latter increases up to a maximum reached for intermediate $\langle LAI \rangle$ values. Indeed, $\langle LAI \rangle$ values that are too low do not allow significant absorption to occur over the domain. Results from Figure 4 also confirm our expectations that tall, clustered and low-density vegetation layers, featured in the medium density canopy condition in Figure 4, constitute difficult cases. They can, indeed, yield $\delta_{A^{1s}}(\mu_0)$ values in the range +0.05 to +0.1 for bright enough background reflectance values, that is, larger than about 0.3 (a scenario occurring when the background is covered by snow, for instance). By contrast, these $\delta_{A^{1s}}(\mu_0)$ values are quite close to zero for environmental conditions where the vegetation layer is bounded by a vegetated understorey. Under diffuse sky illumination, the respective contributions to the fraction of absorbed flux due to the top of the canopy and background albedos are balanced for R_{bgd} values equal to 0.03, 0.04 and 0.46, for the sparse, medium and dense canopy conditions considered in these examples [*Pinty et al.*, 2006, equation (36)].

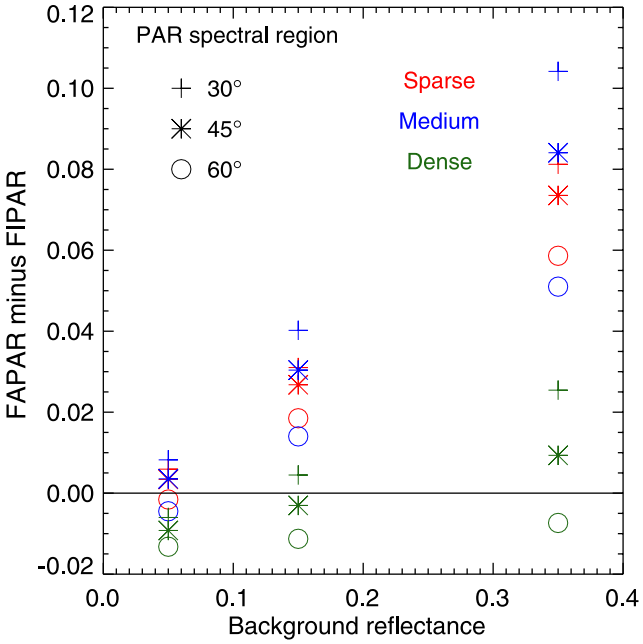

Figure 4. Simulated differences between FAPAR and FIPAR, the term $\delta_{A^{1s}}(\mu_0)$ in (5). Simulations are done for three Sun zenith angle values. They are based on realistic 3-D vegetation scenarios taken from *Pinty et al.* [2006, Tables 1 and 2].

[29] These simulation results suggest that for typical conditions of illumination and background reflectance, the main contribution to FAPAR is given by the intercepted fraction, with respect to both the direct and diffuse illumination. It was shown by *Pinty et al.* [2006, Figure 8] that the contribution to FIPAR due to diffuse sky illumination hardly exceeds +0.03 for typical clear sky conditions. Thus, together with results from Figure 4, one may anticipate that uncertainties due to the contributions from both $\delta_{A^{1s}}(\mu_0)$ and $\overline{\delta_{A^{1s}}}$ can be neglected in the overall uncertainty budget of FAPAR under typical conditions.

[30] The uncertainty of ground estimations of FAPAR, identified with a Δ symbol, can be approximated by

$$\Delta FAPAR^{\star 1s}(\mu_0) \approx \Delta FIPAR(\mu_0) f^{\downarrow dir}(\mu_0) + \Delta \overline{FIPAR} f^{\downarrow diff}(\mu_0). \quad (6)$$

Equation (6) assumes that the relative uncertainty due to the assessment of the fraction of direct versus diffuse radiation is negligible as compared to other sources previously discussed. Thus, according to (4), (6) becomes

$$\Delta FAPAR^{\star 1s}(\mu_0) \approx -\left(\Delta T_{veg}^{UnColl} f^{\downarrow dir}(\mu_0) + \Delta \overline{T_{veg}^{UnColl}} f^{\downarrow diff}(\mu_0)\right). \quad (7)$$

Equations (4) and (7) express the fact that measuring the probability distribution function of the gaps, i.e., T_{veg}^{UnColl}, over the domain constitutes a realistic and technically relatively simple approach for assessing both domain-averaged FAPAR and associated $\Delta FAPAR$ values. Such measurements are indeed feasible thanks to optical field instruments including hemispherical photographs [*Rich*, 1990], the Tracking Radiation and Architecture of Canopies (TRAC) instrument [*Chen and Cihlar*, 1995b], the Burr Brown Data Acquisition System (BBDAS) [*Lang and Yueqin*, 1986] and the LAI-2000 Plant Canopy Analyzer (LI-COR, Lincoln, Nebraska) [*Gower and Norman*, 1991]. Note that the sampling design with any of these instruments will probably be the limiting factor in determining accurate T_{veg}^{UnColl} values over the domain.

[31] Since these instruments are used to measure the total intercepted radiation, their results include a slight contribution from multiple scattering and a contribution from all woody elements, trunk and stems, present within the field of view of the instruments which are looking upward from below the canopy. If the latter contribution is not removed, a very difficult task to perform accurately, these measurements may thus translate into an overestimate of the FIPAR contribution due to leaves only [*Serrano et al.*, 2000]. In order to translate quantitatively, that is, in terms of ΔT_{veg}^{UnColl} values, the relative contribution from woody elements, the domain-averaged direct transmissions were estimated successively with and without a simplified trunk and branching system [*Widlowski et al.*, 2003] for the 3-D heterogeneous canopy scenarios used in section 4.2. For the sparse, medium and dense scenarios, the FIPAR differences are found to be about 0.02 (0.05), 0.03 (0.07), 0.05 (0.02) for a Sun zenith angle of 30° (60°). As one may anticipate given the exponential or power law decay for extinction, the relative contribution due to the woody elements may be especially significant for medium density canopy conditions. A similar range of uncertainty equivalent to ΔT_{veg}^{UnColl} was reported for FIPAR by *J. M. Chen et al.* [1997], when interpreting measurements of gap fractions from in situ optical devices.

[32] The time delays, equivalent to Sun zenith angle differences, between the acquisition of fluxes on the ground and the remote sensing data increase the difficulty when conducting a comparison procedure. Indeed, FIPAR, a good proxy for FAPAR, is dependent on the Sun angle, but, unfortunately, this dependency is a function of the vegetation type, the ambient atmospheric conditions, the day of the year and time of the day, as well as the latitude of the sampled domain. FAPAR thus increases with Sun zenith angle at a rate that changes with $\langle LAI \rangle$ and canopy architecture; these changes are limited for dense canopies (high $\langle LAI \rangle$ values) but can be quite significant for medium dense conditions: For example, *Walter-Shea et al.* [1992] reported diurnal changes in instantaneous FAPAR values of about 0.2 from measurements collected at the First ISLSCP Field Experiment (FIFE) site. For high Sun zenith angles, for example, larger than 60°, the contribution to FAPAR associated with the diffuse sky illumination dampens the increase rate [*Pinty et al.*, 2006, Figure 9]. Therefore canopies that are not subject to seasonal variations in $\langle LAI \rangle$ should logically exhibit a seasonal trend in time-based FAPAR, i.e., higher values in winter than in summer seasons, owing to their dependency with respect to the Sun zenith angle. In the present exercise, this issue will not be quantitatively addressed per se, that is, in terms of ΔT_{veg}^{UnColl}, partly because the needed information is not always available, especially for large-scale (both spatial and temporal) investigations.

4.3. Ground-Based FAPAR Data Sets

[33] To our knowledge, there is no complete data set that permits addressing all caveats discussed in the previous sections, assembling all the needed vertical and horizontal fluxes separately for the direct and diffuse radiation, measured with the appropriate sampling step and at a spatial resolution compatible with the SeaWiFS products, for the same ambient conditions as those prevailing during the acquisition of the remote sensing data. The previous discussion indicates, however, that such an extremely complex set of measurements may not be needed if we are to validate the SeaWiFS FAPAR JRC products within a ±0.1 uncertainty level. Indeed, we have shown that on the basis of model simulations of realistic vegetation canopy scenarios, the compensation between different contributions is such that approximating FAPAR by FIPAR constitutes a first good step in the comparison process.

[34] In the following exercise, we will thus rely only on a limited number of proxy data sets that are available, excluding high-latitude sites for which too few reliable SeaWiFS FAPAR JRC products are available owing to the occurrence of both large Sun zenith angle (larger than assigned in the algorithm training data set) and subpixel snow, water and cloud contamination. Those selected here include either measurements of local and domain-averaged gap fractions and $\langle LAI \rangle$, or combinations of these measurements, and span a wide range of vegetation canopy types which therefore can also be roughly categorized according to their expected or most probable radiation transfer regimes (as deduced from the *Davis and Marshak* [2004] analysis). The latter categorization is based on qualitative knowledge and description of the field sites and not on the detailed analysis of the leaf density distribution function over the domain as should be done, ideally. As suggested from discussions in section 4.1, it first seems appropriate to classify the field sites according to the domain-averaged heights and densities of the prevailing vegetation. This to some extent postulates that these two metrics are inherently linked to their radiation regimes, and serves as the basis for

Table 1. Categorization of Field Validation Sites According to Their Anticipated Radiation Transfer Regimes

Anticipated Radiation Regime[a]	Field Site	Description
Regime 1 "fast variability" short and homogeneous vegetation over 1–2 km	Dahra[b]	semiarid grass savannah
	Tessekre[b]	semiarid grass savannah
	SEVI[c]	desert grassland
Regime 2 "slow variability" mixed vegetation with different land cover types	AGRO[c]	corn and soybean
	HARV[c]	conifer/broadleaf forest
	De Inslag[d]	conifer/broadleaf/shrub forests
	KONZ[c]	grassland/shrubland/cropland
Regime 3 "resonant variability" intermediate height and low-density vegetation	METL[c]	dry needleleaf forest
	Mongu[e]	shrubland/woodland

[a]Based on *Davis and Marshak*'s [2004] analysis.
[b]See *Fensholt et al.* [2004].
[c]See *Turner et al.* [2005].
[d]See *Gond et al.* [1999].
[e]See *Huemmrich et al.* [2005].

designing Table 1. This table lists a series of sites and associated references that will be used below to evaluate the SeaWiFS FAPAR JRC product. A summary of the different approaches adopted to estimate FAPAR values is given in Table 2. The detailed characteristics of the field sites, the size of the sampled domain and the full descriptions of the measuring protocols are available in the publications referred to in Table 1.

[35] Figure 5 shows the time series of the SeaWiFS FAPAR products together with the ground-based estimations available from the five sites, namely, Dahra (15°22′N; 15°26′W), Dahra North (15°24′N; 15°26′W), Tessekre North (15°53′N; 15°3′W), Tessekre South (15°49′N; 15°3′W), and SEVI (34°2′N; 106°42′W), all associated with radiation transfer regime 1, corresponding to the so-called "fast variability" category. The baseline FAPAR value for these sites is close to zero and signatures of the different vegetation phenological cycles (both for the growing and decaying periods) are remarkably well identified by both remote sensing and ground-based estimations. Moreover, the amplitudes, both maxima and minima, are in very good agreement with each other although the remote sensing retrievals tend to slightly underestimate the ground-based values over the site of Dahra during the peak season for 2001 (Figure 5, top left). Incidentally, the landscape at this latter site exhibits some significant spatial heterogeneity at mesoscale which was not sampled by the in situ measurements (and thus was not accounted for in the FAPAR ground-based estimations) but which was probably captured at the resolution available from the SeaWiFS FAPAR products.

[36] Results over vegetation conditions belonging to the "slow variability" category, that is radiation transfer regime 2, are displayed in Figure 6. In the particular case of De Inslag (51°18′N; 4°31′E) (Figure 5, top left), since the ground measurements were collected during year 1997, we have plotted the SeaWiFS FAPAR JRC products for the end of 1997 together with those estimated for 1998, thus assuming that no exceptional event occurred during this period over this site. The amplitudes, that is, the summer maxima and winter minima estimated from both remote sensing and ground measurements, are in very good agreement. The inspection of additional daily instantaneous SeaWiFS products suggests that the year-to-year variations appear to be limited and remain mostly confined within the range of the expected uncertainty of ±0.1, except during the spring period. The ground-based estimated FAPAR values over the agricultural field site identified as AGRO (40°0′N;

Table 2. Outline of the Methodology Adopted for Estimating FAPAR at the Field Validation Sites[a]

Field Site Identification	Summary of the Approach for Domain-Averaged FAPAR Estimations
Dahra	based on BBL's law with measurements of the LAD function; FAPAR(μ_0) derived from the balance between the vertical fluxes; $\langle LAI \rangle$ derived from PCA-LICOR
Tessekre	based on BBL's law with measurements of the LAD function; FAPAR(μ_0) derived from the balance between the vertical fluxes; $\langle LAI \rangle$ derived from PCA-LICOR
SEVI	based on BBL's law with an extinction coefficient equal to 0.5; $\langle LAI \rangle$ derived from specific leaf area data and harvested above ground biomass; advanced procedure to account for spatiotemporal changes of local LAI[b]
AGRO	based on BBL's law with an extinction coefficient equal to 0.5; $\langle LAI \rangle$ from leaf area per plant area and plant density; advanced procedure to account for spatiotemporal changes of local LAI[b]
HARV	based on BBL's law with an extinction coefficient equal to 0.58; $\langle LAI \rangle$ derived from optical PCA-LICOR data; advanced procedure to account for spatiotemporal changes of local LAI[b]
De Inslag	based on full 1-D radiation transfer models; $\langle LAI \rangle$ derived from optical PCA-LICOR data; time-dependent linear mixing procedure weighted by species composition
KONZ	based on BBL's law with an extinction coefficient equal to 0.5; $\langle LAI \rangle$ derived from optical PCA-LICOR data; advanced procedure to account for spatiotemporal changes of local LAI[b]
METL	based on BBL's law with an extinction coefficient equal to 0.5; $\langle LAI \rangle$ derived from optical PCA-LICOR data; advanced procedure to account for spatiotemporal changes of local LAI[b]
Mongu	based on FIPAR estimated from TRAC data; slight contamination by the woody canopy elements; correction to account for the $\delta_{A^{1,*}}(\mu_0)$ contribution (see equation (5))

[a]BBL, Beer-Bouguer-Lambert; LAD, leaf angle distribution.
[b]Extinction coefficient is taken as constant, i.e., independent of the Sun zenith angle.

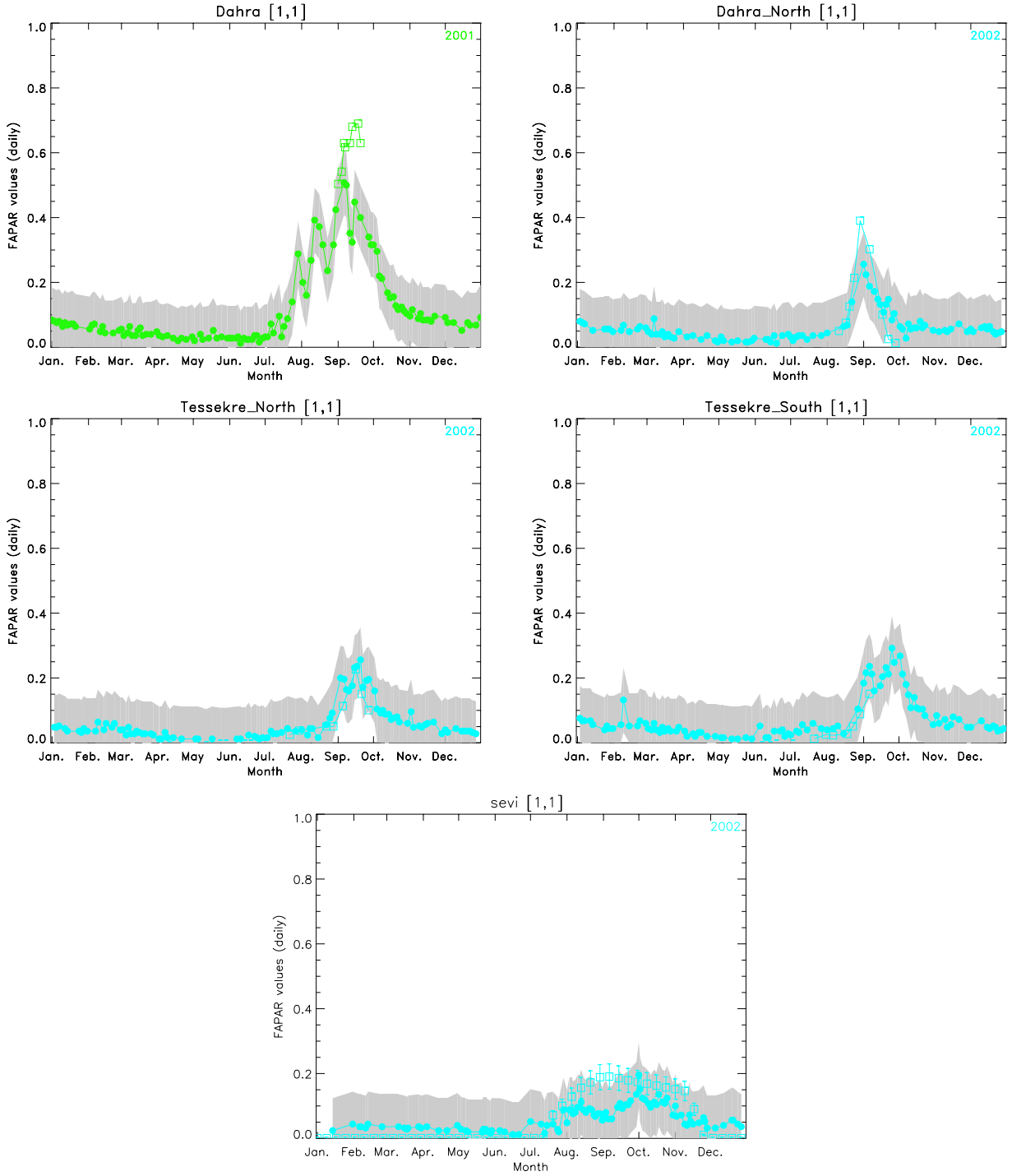

Figure 5. Comparisons of ground-based FAPAR estimations profiles (open squares) and instantaneous daily SeaWiFS FAPAR JRC products (solid circles) over the sites of Dahra, Tessekre, and SEVI associated with radiation transfer regime 1. The zone shaded in gray delineates the ±0.1 uncertainty range around the FAPAR JRC products. The vertical bars indicate the uncertainty range around the ground-based estimations.

88°17′W) follow a well-defined time trajectory that is correctly tracked by the SeaWiFS FAPAR JRC products (Figure 6, top right). We can, however, notice that, on average, the FAPAR maxima and minima from the latter data set tend to be biased high. The third comparison performed with regime 2 canopy conditions, is conducted at the Harvard site (identified as HARV (42°32′N; 72°10′W)), which is a mixture of conifer and hardwood forests. Results from both data sets (Figure 6, bottom left) compare very well with each other for the first 6 months of the year, which includes the growing period. The SeaWiFS FAPAR JRC products then show systematically lower values (about 0.1) than the ground-based estimations during the summer season where vegetation gets very dense over

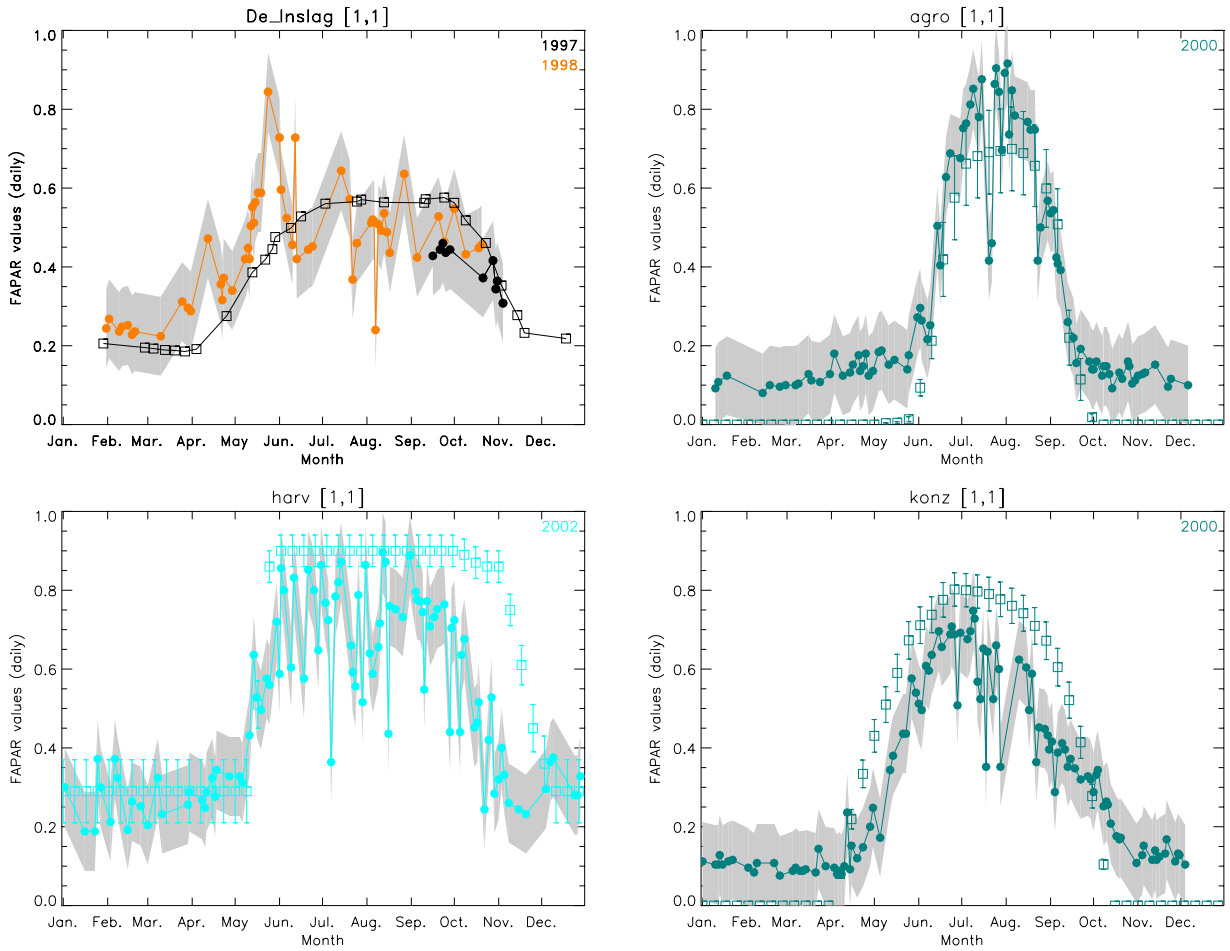

Figure 6. Same as Figure 5 except over the sites of De Inslag, AGRO, HARV, and KONZ associated with radiation transfer regime 2.

the site. The largest discrepancies, however, occur during the senescent period where a time delay of about 1 month is observed between the FAPAR signatures given by the two data sets. The agreement becomes very good again during the winter season, where the FAPAR values are mostly driven by the relative contribution of the vegetation activity of the coniferous patches [*Aber et al.*, 1996]. Both remote sensing and ground-based estimations of FAPAR over the Konza tallgrass prairie site (identified as KONZ [39°4′N; 96°33′W]) indicate the occurrence of a well-marked vegetation seasonal cycle (Figure 6, bottom right). These two estimations are well correlated along the cycle over this site covered by mixed grassland/shrub land and cropland, although the SeaWiFS FAPAR JRC products are slightly biased low. Such a bias occurring during the period of senescence may be a consequence of using total (in ground-based estimations) instead of green (as assumed in the retrieval algorithm) $\langle LAI \rangle$ values when assessing the FAPAR values. The differences in both $\langle LAI \rangle$ values could indeed be somewhat significant, as reported for instance, by *T. H. Chen et al.* [1997].

[37] The high patchiness of the medium resolution domains, investigated in the case of vegetation canopies associated with regime 2, and the uncertainties inherent in the geographical colocation of the field sites and the remote sensing products, decrease the probability of comparing the radiant fluxes precisely enough over the same domains. This is a reasonable argument to be invoked when dealing with a quite spatially and temporarily changing environment sampled with a medium resolution space sensor. However, given the quite complex procedures involved in the assessment of the ground-based FAPAR values, various other factors, including the Sun zenith angle effects, could also explain some of the observed biases and discrepancies when occasionally larger than ±0.1.

[38] The results of this comparison exercise for vegetation conditions associated with regimes 1 and 2 are summarized in Figure 7 (based on 10-day composite values). It shows that, generally, the FAPAR values retrieved from a medium resolution space sensor are well within the specified uncertainty range of ±0.1, when directly compared to a series of available ground-based proxy data sets for FAPAR. Given the many sources of sometimes uncontrolled uncertainties and errors that are contaminating this comparison exercise (some of them yielding deviations as large as 0.4), we can consider that Figure 7 displays quite encouraging results for both the remote sensing and ground-based estimations.

[39] The comparison results of ground-based and SeaWiFS retrieved FAPAR over the METL site (44°26′N; 121°34′W), associated with regime 3 are shown in Figure 8 (top). The two main interesting features are that (1) both sources of information indicate the absence of a

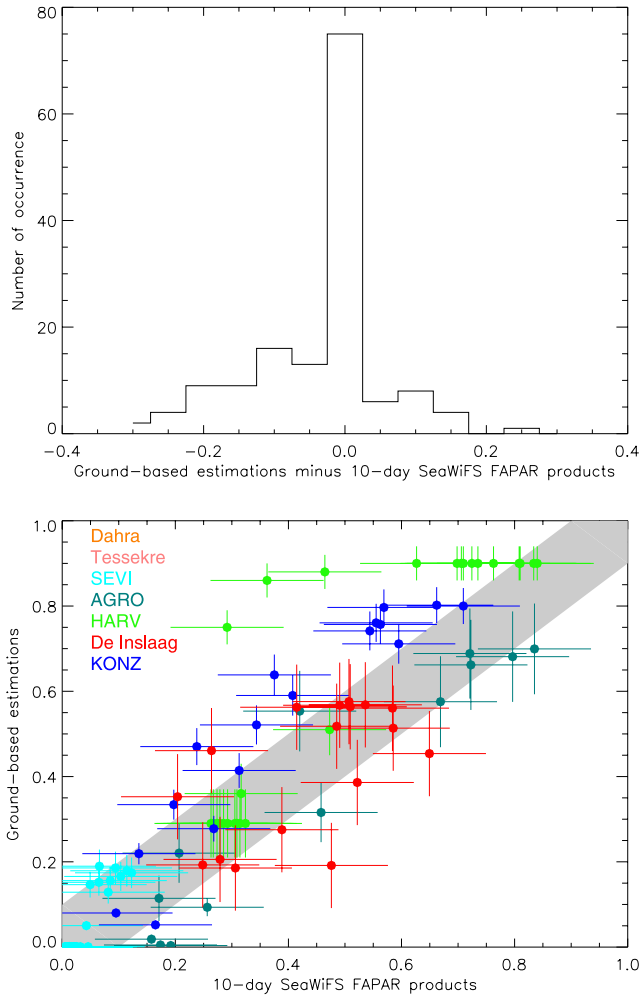

Figure 7. (top) Histogram of the differences and (bottom) scatterplot of the ground-based and 10-day composite SeaWiFS FAPAR values over all sites associated with radiative transfer regimes 1 and 2. Note that SeaWiFS FAPAR values assessed for both years 1997 and 1998 are used in the particular case of De Inslag. The zone shaded in gray delineates the ±0.1 uncertainty range. The vertical (horizontal) bars indicate the uncertainty range around the ground-based estimations (SeaWiFS FAPAR values).

strong seasonal cycle, as could be expected over this ponderosa pine conifer forest, and (2) the discrepancy in the FAPAR amplitudes between the two data sets is extremely high (about a factor of 2). Interestingly, this is a typical class of canopies deviating significantly from the 1-D statistically homogeneous situation. In that instance, the classical Beer-Bouguer-Lambert law of exponential attenuation applies only if the 3-D radiative effects are adequately parameterized. As shown by *Pinty et al.* [2006], all radiant fluxes including FAPAR can be retrieved accurately if effective instead of true domain-averaged state variables are adopted. To do so, *Pinty et al.* [2006] have proposed inferring a structure factor, $\zeta(\mu_0)$, defined with respect to the domain-averaged transmission factor, $\langle T_{veg}^{UnColl}(\mu_0)\rangle$,

$$\left\langle T_{veg}^{UnColl}(\mu_0)\right\rangle = \exp\left(-\widetilde{LAI}(\mu_0)/2\,\mu_0\right), \tag{8}$$

with

$$\widetilde{LAI}(\mu_0) = \langle LAI\rangle\,\zeta(\mu_0), \tag{9}$$

where $\widetilde{LAI}(\mu_0)$ denotes the effective LAI, a domain-averaged quantity which differs from the true or allometric $\langle LAI\rangle$ by a factor embedding a number of effects associated with the 3-D heterogeneous structure of the vegetation. *Chen and Cihlar* [1995a] have reached a similar conclusion regarding the estimate of the direct transmitted flux, and they adopted a factor defined explicitly as a function of parameters representing the foliage clumping and the wood-related contribution to the extinction of solar radiation.

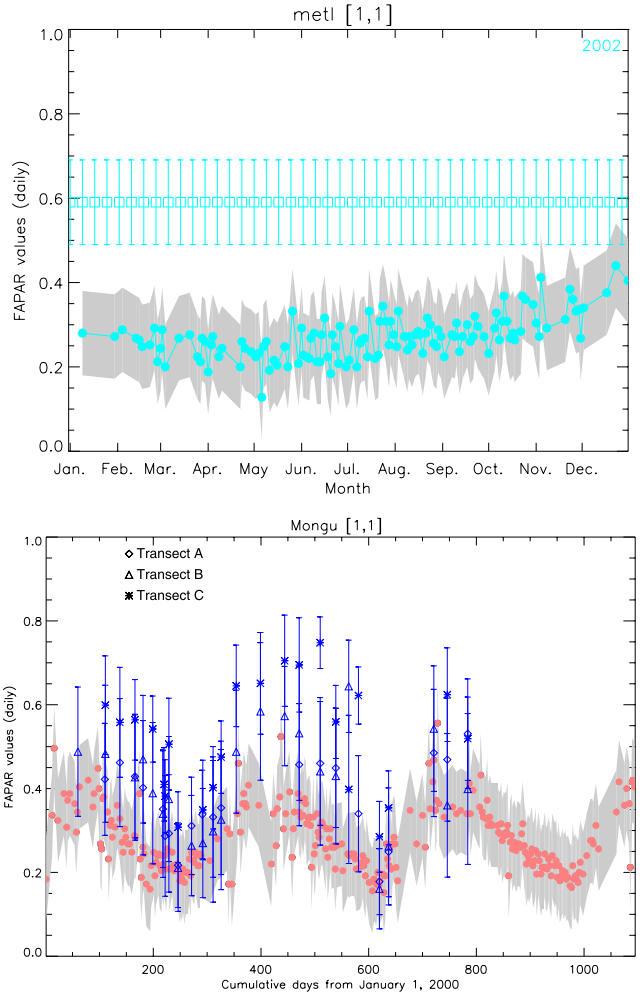

Figure 8. (top) Comparisons of ground-based FAPAR estimations profiles (open squares) and instantaneous daily SeaWiFS FAPAR JRC products (solid circles) over the site METL associated with radiative transfer regime 3. (bottom) Same as above except over the Mongu site. The ground-based estimations over the three transects marked A, B, and C are identified with diamonds, triangles, and asterisks, respectively. The zone shaded in gray delineates the ±0.1 uncertainty range around the FAPAR JRC products. The vertical bars indicate the uncertainty range around the ground-based estimations.

[40] The $\zeta(\mu_0)$ factor in (9) thus forces the direct radiation to be intercepted, on average over the domain, with statistical rules identical to those prevailing in the case of 1-D homogenous canopies, assuming a spherical leaf angle distribution function which implies a leaf extinction coefficient equal to 0.5. This factor is thus equal to unity for 1-D homogeneous canopies only. Adopting a value equal to unity for estimating the FAPAR from in situ information over the METL site [*Turner et al.*, 2005] corresponds to an assumption that may therefore significantly contribute to the discrepancy between the ground-based and satellite retrieved FAPAR values over this site. The values of the $\zeta(\mu_0)$ structure factor that would provide the optimal fit between the ground-based and the satellite-derived FAPAR value range between 0.5 and 0.6. Incidentally, such values are similar to those simulated with a 3-D model for a medium-density conifer forest having an allometric $\langle LAI \rangle$ equal to 2.0 [*Pinty et al.*, 2006, Figure 2]. It is also noteworthy that such values for $\zeta(\mu_0)$ are consistent with those measured in situ during the international Boreal Ecosystem-Atmosphere Study (BOREAS) [*Chen and Cihlar*, 1995a, p. 782]. Indeed, these authors reported an effective LAI value of about 1.5 over a young jack pine forest for which allometric $\langle LAI \rangle$ is equal to 2.8. In turn, this reduction in LAI values entering the 1-D extinction scheme significantly affects the ground-based estimated FIPAR. Results for this simple analysis therefore suggest that the SeaWiFS FAPAR JRC products could actually well be in the range to be expected for this type of 3-D structured low-density conditions. Clearly, similar effects could also partly explain some of the discrepancies observed over other sites where some 3-D heterogeneity exist. The specific case of METL is especially interesting since, by contrast to other sites, these 3-D induced effects are not smeared out by strong seasonal cycles.

[41] The additional ground-based data set associated with regime 3, identified in Table 1 as Mongu (15°26′S; 23°15′E), derives from a careful collection and analysis of the canopy gap fraction using the TRAC instrument over two consecutive years in a mixed shrubland/woodland environment. Figure 8 (bottom) thus shows the time series of the SeaWiFS FAPAR JRC products for years 2000 to 2002 together with the interpreted measurements (in terms of FAPAR spatial averages and associated standard deviations) collected by the TRAC instrument over three transects of 750 m at a spatial resolution of about 1.7 cm. These data include a numerically small (as confirmed by our model simulations shown in Figure 4) correction to account for the $\delta_{A^{1s}}(\mu_0)$ contributions. During the two wet seasons, that is, approximately from September to January, the agreement between the SeaWiFS and ground-based estimations is very good. By contrast, SeaWiFS FAPAR JRC products are systematically biased low, by about 0.1 on average, during the two dry seasons, although the uncertainty ranges of both estimations do overlap and the correlation between the two estimations always remains quite high. The ground-based estimations report FAPAR values for 2001 that slightly exceed those from the previous year, leading to an enhancement of the observed bias. The discrepancies are also generally higher in the case of transect C, corresponding to denser canopy conditions, than with transects A and B. On the positive side, one may keep in mind that the remaining contamination of the FIPAR measurements by the woody (nongreen) elements of the canopy favors the occurrence of such a bias with respect to the SeaWiFS FAPAR values. This feature is expected to be enhanced during the dry season when the relative contribution to the extinction process by the leaves only is decreasing, especially with such a low-density canopy (the $\langle LAI \rangle$ varies approximately in the range [1−1.5] during the dry seasons [*Privette et al.*, 2004]). Much more advanced investigations including, for instance, the Sun angle effects and the 3-D modeling of such vegetation scenarios, must be carried out to better understand the observed discrepancies and thus reduce the specified uncertainty range on the SeaWiFS FAPAR JRC products.

5. Conclusions

[42] This paper presents the results of an evaluation of the quality of the SeaWiFS FAPAR JRC products available from September 1997 up to year 2004. This assessment is achieved in two complementary phases: (1) The verisimilitude of the products is examined over selected sites that exhibit different land cover types and that were exposed to some significant level of stress during the 6-year time series, and (2) the FAPAR values are directly compared against ground-based estimations over specific sites where field investigations have been carried out.

[43] The first phase emphasizes the analysis of seasonal cycles and the inter-annual variations shown by the FAPAR products. It was found that these seasonal and year-to-year variations are, as expected, strongly affected when significant environmental stress conditions happen, such as those associated with the occurrence of the 2003 European drought and the intense fires in Oregon during summer 2002. The FAPAR signatures are indeed well marked and exceed the prespecified ±0.1 accuracy range. By contrast, the FAPAR time series are not significantly different in the absence of such drastic events. The results presented here therefore support the hypothesis that FAPAR can be used as an indicator to monitor the presence and health of vegetation globally at medium spatial resolution. A FAPAR algorithm, analogous to the one designed for the SeaWiFS sensor, is currently operated by the European Space Agency (ESA) in order to deliver products from the MERIS sensor. Since the SeaWiFS and MERIS FAPAR products are equivalent, they can be used interchangeably and merged together to ensure a better spatiotemporal coverage and a continuous data stream.

[44] Despite the number of complex theoretical and technical issues and caveats to be faced, the present comparison exercise of satellite-derived FAPAR products against ground-based estimations uses the available in situ measurements. Three-dimensional radiation transfer model simulations are used to evaluate the contributions to the FAPAR balance equation that are generally not measured in situ. It was shown that, fortunately, and except under particular circumstances, the fraction of intercepted radiation, FIPAR, is a good proxy for FAPAR, in the sense that the numerical differences between these two fluxes, intercepted and absorbed, are often confined within the ±0.1 FAPAR accuracy range. A categorization of the different sites where FAPAR field data sets are available, based on

the anticipated radiative transfer regimes, is used to better identify and thus recognize the level of difficulties to be faced from both technical and theoretical perspectives.

[45] This categorization recognizes that the degree of three-dimensional internal variability of the leaf density over the different vegetation types sampled in situ translates into different radiative transfer regimes. They are themselves critical when analyzing the results of the comparison, in the sense that the main sources of uncertainties or discrepancies between the remote sensing and in situ data sets probably differ between the various radiative transfer regimes prevailing at the concerned spatial resolutions. In the case of short and spatially homogenous vegetation (regime 1), one may anticipate that the main source of discrepancies is dominated by sampling time difference which involves the coupled effect between the Sun zenith angle and actual leaf angle distribution function. When the radiative transfer regime is mostly controlled by the mixture of multiple vegetation types exhibiting different phenological behavior (regime 2) geo-location uncertainties and pixel size may be the main issues in performing a reliable and accurate comparison exercise. Under conditions of intermediate but low-density vegetation canopies (regime 3), effects associated with the canopy structure and the presence of woody elements significantly contribute to the quality assessment of the FAPAR values.

[46] Overall, the comparison results are encouraging since the SeaWiFS FAPAR JRC products behave as can be expected given the difficulties associated with each regime mentioned above. The FAPAR products appeared biased low with respect to the ground-based estimations especially under conditions where the structural effects become significant and/or the contribution of the woody elements of the canopy to the interception process is not negligible. The FAPAR products often display, however, a quite good representation of the seasonal cycles as inferred from ground-based estimations.

[47] An IDL and C version of the FAPAR algorithm can be requested from the first author by sending a message to nadine.gobron@jrc.it. The SeaWiFS FAPAR JRC products are available at the following address: http://fapar.jrc.it.

[48] **Acknowledgments.** The authors are grateful to the SeaWiFS Project (Code 970.2) and the Distributed Active Archive Center (Code 902) at the NASA Goddard Space Flight Center, Greenbelt, MD 20771, for the production and distribution of the SeaWiFS data, respectively. Part of this work has been carried out in the frame of CarboEurope Integrated Project, supported by the European Commission, Directorate-General Research, 6th Framework Programme, under contract GOCE-CT-2003-505572. Linda Hunt and Anthony B. Davis kindly commented on an early draft.

References

Aber, J. D., P. B. Reich, and M. L. Goulden (1996), Extrapolating leaf CO_2 exchange to the canopy: A generalized model of forest photosynthesis validated by eddy correlation, *Oecologia*, *106*, 267–275.

Brown, M., G. G. Parker, and N. E. Posner (1994), A survey of ultraviolet-B radiation in forest, *J. Ecol.*, *82*, 843–854.

Chen, J. M., and J. Cihlar (1995a), Quantifying the effect of canopy architecture on optical measurements of leaf area index using two gap size analysis methods, *IEEE Trans. Geosci. Remote Sens.*, *33*, 777–787.

Chen, J. M., and J. Cihlar (1995b), Plant canopy gap size analysis theory for improving optical measurements of leaf area index, *Appl. Opt.*, *34*, 6211–6222.

Chen, J. M., P. M. Rich, S. T. Gower, J. M. Norman, and S. Plummer (1997), Leaf area index of boreal forests: Theory, techniques, and measurements, *J. Geophys. Res.*, *102*, 29,429–29,443.

Chen, T. H., et al. (1997), Cabauw experimental results from the project for intercomparison of land-surface parameterization schemes, *J. Clim.*, *10*, 1194–1215.

Comeau, P. G., F. Gendron, and T. Letchford (1998), A comparison of several methods for estimating light under a paper birch mixewood stand, *Can. J. For. Res.*, *28*, 1843–1850.

Davis, A. B., and A. Marshak (2004), Photon propagation in heterogeneous optical media with spatial correlations: Enhanced mean free-paths and wider-than-exponential free-path distributions, *J. Quant. Spectrosc. Radiat. Transfer*, *84*, 3–34.

Fensholt, R., I. Sandholt, and M. S. Rasmussen (2004), Evaluation of MODIS LAI, fAPAR and the relation between fAPAR and NDVI in a semi-arid environment using in situ measurements, *Remote Sens. Environ.*, *91*, 490–507.

Gobron, N., B. Pinty, M. M. Verstraete, and Y. Govaerts (1999), The MERIS Global Vegetation Index (MGVI): Description and preliminary application, *Int. J. Remote Sens.*, *20*, 1917–1927.

Gobron, N., B. Pinty, M. M. Verstraete, and J.-L. Widlowski (2000), Advanced spectral algorithm and new vegetation indices optimized for up coming sensors: Development, accuracy and applications, *IEEE Trans. Geosci. Remote Sens.*, *38*, 2489–2505.

Gobron, N., F. Mélin, B. Pinty, M. M. Verstraete, J.-L. Widlowski, and G. Bucini (2001), A global vegetation index for SeaWiFS: Design and applications, in *Remote Sensing and Climate Modeling: Synergies and Limitations*, edited by M. Beniston and M. M. Verstraete, pp. 5–21, Springer, New York.

Gobron, N., B. Pinty, F. Mélin, M. Taberner, and M. M. Verstraete (2002), Sea Wide Field-of-View Sensor (SeaWiFS) - Level 2 land surface products—Algorithm theoretical basis document, *EUR Rep. 20144 EN*, Inst. for Environ. and Sustainability, Ispra, Italy.

Gobron, N., B. Pinty, F. Mélin, M. Taberner, M. M. Verstraete, A. Belward, T. Lavergne, and J.-L. Widlowski (2005), The state of vegetation in Europe following the 2003 drought, *Int. J. Remote Sens. Lett.*, *26*, 2013–2020.

Gobron, N., B. Pinty, F. Mélin, M. Taberner, M. Verstraete, M. Robustelli, and J.-L. Widlowski (2006), Evaluation of the MERIS/ENVISAT fAPAR product, *Adv. Space Res.*, *37*, doi:10.1016/j.asr.2006.02.048.

Gond, V., D. G. G. de Pury, F. Veroustraete, and R. Ceulemans (1999), Seasonal variations in leaf area index, leaf chlorophyll, and water content; Scaling-up to estimate fAPAR and carbon balance in a multilayer, multi-species temperate forest, *Tree Physiol.*, *19*, 673–679.

Govaerts, Y., M. M. Verstraete, B. Pinty, and N. Gobron (1999), Designing optimal spectral indices: A feasibility and proof of concept study, *Int. J. Remote Sens.*, *20*, 1853–1873.

Gower, S. T., and J. M. Norman (1991), Rapid evolution of leaf area index in conifer and broad-leaf plantations, *Ecology*, *72*, 1896–1900.

Hooker, S., W. Esaias, G. Feldman, W. Gregg, and C. McClain (1992), An overview of SeaWiFS and ocean color, *NASA Tech. Memo., 104566*, 24 pp.

Huemmrich, K. F., J. L. Privette, M. Mukelabai, R. B. Myneni, and Y. Knyazikhin (2005), Time-series validation of MODIS land biophysical products in a Kalahari woodland, Africa, *Int. J. Remote Sens.*, *26*, 4381–4398.

Kaufman, Y. J., A. Wald, L. Remer, B. Gao, R. Li, and L. Flynn (1997), Remote sensing of aerosol over the continents with the aid of the 2.2 μm channel, *IEEE Trans. Geosci. Remote Sens.*, *35*, 1286–1298.

Kaufman, Y. J., N. Gobron, B. Pinty, J.-L. Widlowski, and M. M. Verstraete (2002), Relationship between surface reflectance in the visible and mid-IR used in MODIS aerosol algorithm, *Geophys. Res. Lett.*, *29*(23), 2116, doi:10.1029/2001GL014492.

Knorr, W., N. Gobron, M. Scholze, T. Kaminski, and B. Pinty (2005), Global drought conditions causing recent atmospheric carbon dioxide increase, *Eos Trans. AGU*, *86*, 178,181.

Knyazikhin, Y., J. V. Martonchik, D. J. Diner, R. B. Myneni, M. M. Verstraete, B. Pinty, and N. Gobron (1998a), Estimation of vegetation canopy leaf area index and fraction of absorbed photosynthetically active radiation from atmosphere-corrected MISR data, *J. Geophys. Res.*, *103*, 32,239–32,256.

Knyazikhin, Y., J. V. Martonchik, R. B. Myneni, D. J. Diner, and S. W. Running (1998b), Synergistic algorithm for estimation of vegetation canopy leaf area index and fraction of absorbed photosynthetically active radiation from MODIS and MISR data, *J. Geophys. Res.*, *103*, 32,257–32,276.

Lang, A. R. G., and X. Yueqin (1986), Estimation of leaf area index from transmission of direct sunlight in discontinuous canopies, *Agric. For. Meteorol.*, *37*, 229–243.

Lewis, P., and M. Barnsley (1994), Influence of the sky radiance distribution on various formulations of the Earth surface albedo, paper presented at 6th ISPRS International Symposium on Physical Measurements and Signatures in Remote Sensing, Cent. Natl. d'Etudes Spatiales, Val d'Isère, France.

Martonchik, J. V., D. J. Diner, R. A. Kahn, T. P. Ackerman, M. M. Verstraete, B. Pinty, and H. R. Gordon (1998), Techniques for the retrieval of aerosol properties over land and ocean using multi-angle imaging, *IEEE Trans. Geosci. Remote Sens.*, *36*, 1212–1227.

Mélin, F., C. Steinich, N. Gobron, B. Pinty, and M. Verstraete (2002), Optimal merging of LAC and GAC data from SeaWiFS, *Int. J. Remote Sens.*, *23*, 801–807.

Nicotra, A., R. Chazdon, and S. V. B. Iriarte (1999), Spatial heterogeneity of light and woody seedling regeneration in tropical wet forests, *Ecology*, *80*, 1908–1926.

Parker, G. G. (1995), Structure and microclimate of forest canopies, in *A Review of Research on a Biological Frontier*, edited by M. Lowman and N. Nadkami, pp. 73–106, Elsevier, New York.

Pinty, B., N. Gobron, F. Mélin, and M. M. Verstraete (2002), A time composite algorithm theoretical basis document, *EUR Rep. 20150 EN*, Inst. for Environ. and Sustainability, Ispra, Italy.

Pinty, B., A. Lattanzio, J. V. Martonchik, M. M. Verstraete, N. Gobron, M. Taberner, J.-L. Widlowski, R. E. Dickinson, and Y. Govaerts (2005), Coupling diffuse sky radiation and surface albedo, *J. Atmos. Sci.*, *62*, 2580–2591.

Pinty, B., T. Lavergne, R. E. Dickinson, J.-L. Widlowski, N. Gobron, and M. M. Verstraete (2006), Simplifying the interaction of land surfaces with radiation for relating remote sensing products to climate models, *J. Geophys. Res.*, *111*, D02116, doi:10.1029/2005JD005952.

Pitman, A. (2003), The evolution of, and revolution in, land surface schemes designed for climate models, *Int. J. Climatol.*, *23*, 479–510.

Privette, J. L., Y. Tian, G. Roberts, R. Scholes, Y. Wang, K. K. Caylor, P. Frost, and M. Mukelabai (2004), Vegetation structure characteristics and relationships of Kalahari woodlands and savannas, *Global Change Biol.*, *10*, 281–291.

Rich, P. M. (1990), Characterizing plant canopies with hemispherical photographs: Instrumentation for studying vegetation canopies for remote sensing in optical and thermal infrared regions, *Remote Sens. Rev.*, *5*, 13–29.

Sellers, P. J., et al. (1997), Modeling the exchanges of energy, water, and carbon between continents and the atmosphere, *Science*, *275*, 502–509.

Serrano, L., J. A. Gamon, and J. Peñuelas (2000), Estimation of canopy photosynthetic and nonphotosynthetic components from spectral transmittance, *Ecology*, *81*, 3149–3162.

Shabanov, N. V., Y. Wang, W. Buermann, J. Dong, S. Hoffman, G. R. Smith, Y. Tian, Y. Knyazikhin, and R. B. Myneni (2003), Effect of foliage spatial heterogeneity in the MODIS LAI and FPAR algorithm over broadleaf forests, *Remote Sens. Environ.*, *85*, 410–423.

Steering Committee for GCOS (2003), Summary report of the eleventh session of the WMO-IOC-UNEP-ICSU, *WMO/TD 1189*, World Meteorol. Org., Melbourne, Australia.

Turner, D. P., et al. (2005), Site-level evaluation of satellite-based global terrestrial gross primary production and net primary production monitoring, *Global Change Biol.*, *11*, 666–684.

Verstraete, M. M., and B. Pinty (1996), Designing optimal spectral indices for remote sensing applications, *IEEE Trans. Geosci. Remote Sens.*, *34*, 1254–1265.

Walter-Shea, E. A., B. L. Blad, C. J. Hays, M. A. Mesarch, D. W. Deering, and E. M. Middleton (1992), Biophysical properties affecting vegetative canopy reflectance and absorbed photosynthetically active radiation at the FIFE site, *J. Geophys. Res.*, *97*, 18,925–18,934.

Wang, Q., S. Adiku, J. Tenhunen, and A. Granier (2005), On the relationship of NDVI with leaf area index in a deciduous forest site, *Remote Sens. Environ.*, *94*, 244–255.

Wang, Y., et al. (2004), Evaluation of the MODIS LAI algorithm at a coniferous forest site in Finland, *Remote Sens. Environ.*, *91*, 114–127.

Widlowski, J.-L., M. M. Verstraete, B. Pinty, and N. Gobron (2003), Allometric relationships of selected European tree species, *Rep. EUR 20855 EN*, Joint Res. Cent., Ispra, Italy.

Widlowski, J.-L., B. Pinty, T. Lavergne, M. M. Verstraete, and N. Gobron (2005), Using 1-D models to interpret the reflectance anisotropy of 3-D canopy targets: Issues and caveats, *IEEE Trans. Geosci. Remote Sens.*, *43*, 2008–2017.

Widlowski, J.-L., B. Pinty, T. Lavergne, M. M. Verstraete, and N. Gobron (2006), Horizontal radiation transport in 3-d forest canopies at multiple spatial resolutions: Simulated impact on canopy absorption, *Remote Sens. Environ.*, *101*, doi:10.1016/j.rse.2006.03.014.

O. Aussedat, N. Gobron, T. Lavergne, F. Mélin, B. Pinty, M. Taberner, M. M. Verstraete, and J.-L. Widlowski, Global Environmental Monitoring Unit, IES, European Commission Joint Research Centre, TP 440, via E. Fermi, I-21020 Ispra (VA), Italy. (nadine.gobron@jrc.it)

J. M. Chen, Department of Geography and Program in Planning, University of Toronto, 100 Saint George Street, Toronto, ON, Canada M5S 3G3.

W. B. Cohen, USDA Forest Service, 3200 SW Jefferson Way, Corvallis, OR 97331, USA.

R. Fensholt and I. Sandholt, Institute of Geography, University of Copenhagen, Østen Voldgrade 10, DK-1350 Copenhagen, Denmark.

V. Gond, Forest Department, Centre de Coopération Internationale en Recherche Agronomique pour le Développement, 97323 Cayenne, French Guyana.

K. F. Huemmrich, Joint Center for Earth System Technology, University of Maryland Baltimore County, Baltimore, MD 21250, USA.

J. L. Privette, NASA Goddard Space Flight Center, Code 614.4, Greenbelt, MD 20771, USA.

D. P. Turner, Department of Forest Science, Oregon State University, Corvallis, OR 97331, USA.